Calorimetry of Photon Gases in Nonlinear Multimode Optical Fibers

M. Ferraro,[1,*] F. Mangini,[1,*,†] F. O. Wu,[2] M. Zitelli,[1] D. N. Christodoulides,[2] and S. Wabnitz[1,3]

[1]*Department of Information Engineering, Electronics, and Telecommunications, Sapienza University of Rome, Via Eudossiana 18, 00184 Rome, Italy*

[2]*CREOL-College of Optics and Photonics, University of Central Florida, Orlando, Florida 32816, USA*

[3]*CNR-INO, Istituto Nazionale di Ottica, Via Campi Flegrei 34, 80078 Pozzuoli, Italy*

(Received 27 November 2022; accepted 11 December 2023; published 29 April 2024)

Recent studies have shown that light propagating in a nonlinear, highly multimode system can thermalize in a manner totally analogous to that encountered in traditional statistical mechanics. At thermal equilibrium, the system's entropy is at a maximum, in full accord with the second law of thermodynamics. In such arrangements, the entropy is extremized once the statistical power allocation among modes associated with this photon gas attains a Rayleigh-Jeans distribution that is fully characterized by an optical temperature T and a chemical potential μ. However, it has been theoretically argued that the variables T and μ represent actual thermodynamic forces that control the exchange of the respective conjugate quantities between two subsystems. In this work, we report, for the first time, optical calorimetric measurements in nonlinear multimode fibers, which unambiguously demonstrate that both the temperature T and the chemical potential μ dictate the flow of their associated extensive quantities, i.e., the energy and the optical power. Specifically, we study the process of light thermalization associated with two orthogonally polarized laser beams. Our observations are enabled by recently developed techniques that allow one to judiciously multiplex/demultiplex the optical power within various mode groups. Our results indicate that because of photon-photon collisions, "heat" only flows from a hot to a cold photon gas subsystem—thus providing an unequivocal demonstration of the second law in such all-optical thermodynamic arrangements. In addition to being fundamental, our findings provide a new approach to manipulate laser beams using thermodynamic principles.

DOI: 10.1103/PhysRevX.14.021020

Subject Areas: Nonlinear Dynamics, Optics, Statistical Physics

I. INTRODUCTION

In classical physics, optical and thermodynamic phenomena are generally categorized into two distinct classes, given that the former is ruled by Maxwell's equations while the latter follows the principles of statistical mechanics. Although thermodynamic effects merge with optics when light interacts with matter—e.g., polariton condensates in semiconductors, dye-filled optical microcavities [1,2], and plasmonic resonances in metallic nanostructures [3]—these same processes are completely absent in purely linear optical systems due to the very nature of photons. Nevertheless, in nonlinear optical settings, photons can interact with each other through a variety of conservative nonlinear mechanisms, which is in great contrast to linear environments where superposition is allowed; hence, electromagnetic waves recover their initial state once their interference ends. In the nonlinear domain, electromagnetic waves do not simply interfere, but they may experience a nontrivial, utterly complex interaction that completely alters their state [4]. To understand such convoluted interactions in multimode nonlinear systems, a series of attempts were made to establish a statistical description of these effects [5–11]. Yet, a self-consistent thermodynamic theory was put forward recently to understand, explain, predict, and harness these complex nonlinear chaotic processes in highly multimode nonlinear environments [12].

In this theoretical framework, a multimode nonlinear arrangement is shown to exhibit a behavior akin to that of a gas of particles. In this respect, the photon occupancies, assigned to each mode, vary during nonlinear propagation—an aspect that leads to energy exchange via particle or "photon-photon" collisions. Eventually, the mode occupancy distribution reaches thermal equilibrium, which corresponds to a state of maximum entropy (S), as expected from the second law of thermodynamics. In this case, the distribution at equilibrium is described by the Rayleigh-Jeans

[*]These authors have contributed equally to this work.

[†]Corresponding author: fabio.mangini@uniroma1.it

(RJ) law, once the modes are sorted through their propagation constants. The resulting RJ distribution is completely characterized by a temperature (T) and a chemical potential (μ), which specify the state at thermal equilibrium. In general, the two intensive parameters T and μ can be uniquely determined from initial conditions [13,14], through an equation of state in a way analogous to thermodynamic gases [15], where T and μ are linked to the extensive invariant parameters of the system. They are as follows: (i) the optical Hamiltonian, which is related to conserved linear momentum of the system and is hereafter called internal energy (U); (ii) the optical power ($\mathcal{P}$) in the system (which is also conserved in a lossless arrangement), which plays the role of the number of particles; and (iii) the number of modes supported by the systems, which corresponds to the volume that is accessible to the photon gas (M). This overarching equation of state is given by [12]

$$U - \mu\mathcal{P} = MT. \tag{1}$$

We note that this theoretical framework is universal and applies to any type of nonlinear multimode system in the weakly nonlinear regime [13,16,17]. Recently, its validity has been experimentally confirmed in multimode optical fibers (MMFs) [18,19]. When applied to the relevant case of graded-index MMFs, this thermodynamic description allows one to explain and understand the intricacies behind the so-called beam self-cleaning effect, whereby a highly speckled beam morphs into a bell-shaped wavefront because of nonlinearity [20,21]. In recent years, this phenomenon has attracted much attention, owing to its potential relevance for applications, e.g., for developing high-energy fiber lasers [22,23] and high-resolution imaging devices [24].

It is in this context that the new thermodynamic framework displays its true potential, given that one can predict the final modal composition at the fiber output from the mere knowledge of the input beam state, without resorting to heavy numerical simulations that are computationally both time- and energy-consuming. In this regard, it is important to note that the values of T and μ are fully determined by the input launching conditions, i.e., when the laser source excites the MMF. Therefore, in practical settings, the temperature and the chemical potential of a beam can be varied by simply introducing a small angle between the direction of the laser beam and the fiber axis [25], as well as by appropriately modifying the laser wavefront [26]. Generally speaking, the lower one sets the beam temperature, the "cleaner" and brighter the thermalized beam will appear at the output. In other words, if the optical temperature is low enough, only the fundamental mode, i.e., the mode having the highest propagation constant, will be macroscopically populated at equilibrium—a phenomenon corresponding to classical wave condensation [27,28].

Here, we focus on demonstrating a crucial prediction of optical thermodynamics [12]. Specifically, in analogy with other thermodynamic quantum systems [29], we extend the theoretical study of classical nonlinear optical gases by deploying calorimetric methods. At variance with Ref. [29], which uses a single gas of photons whose temperature is varied by an external source of heat, in this work, we examine the process of heat transfer between two photon (of orthogonal polarization) gases when propagating in an MMF, which is thermally insulated. We find that the interaction between the gases leads to a new state of thermal equilibrium, whose parameters (temperature and chemical potential) are fully determined by the initial conditions (T_1, μ_1; T_2, μ_2) of the two gases, when considered separately. In this regime, the two subsystems thermodynamically interact in a grand-canonical-like manner; i.e., they are allowed to exchange both power and energy (momentum). This process has never been observed experimentally in any study so far, partly due to the fact that, for many years, no physical significance was attributed to the intensive variables T and μ, and the respective optical entropy S. In particular, it is only because of entropy maximization that the heat flows from hot to cold systems, in full accord with the second law. Indeed, the second law of thermodynamics dictates that entropy maximization can only allow energy flow from hot to cold, while it prohibits a converse scenario. In this sense, the calorimetric study of photon gases allows one to unambiguously demonstrate that the optical entropy associated with multimode nonlinear systems is not only physical but also fully analogous to the entropy in standard thermodynamic formalisms. We show that our theoretical predictions are fully confirmed by experiments that rely on the holographic mode decomposition technique [30].

Indeed, our findings imply that it is possible to modify the quality or brightness of a laser beam by exploiting the nonlinear interaction with another beam in an MMF that happens to have either a higher or lower temperature. In this sense, our results pave the way for developing a new generation of photonic tools for all-optically controlling the spatial profile of intense laser beams.

II. THEORETICAL FRAMEWORK

Thermodynamics rules the properties of gases at thermal equilibrium and permits their description in terms of macroscopic parameters such as M, $\mathcal{P}$, μ, and T [12,31]. The study of thermodynamic processes under quasi- or nonequilibrium conditions by, e.g., the exposition of a given object to an external heat source, or via a phase transition, is the key topic of calorimetry. Temperature is one of the first quantities that is introduced in a thermodynamic theory: In statistical mechanics, it is defined in purely mathematical terms—it describes the microscopic distribution of particles among various kinetic energy levels, or, in the case of a photon gas, its modal occupancy.

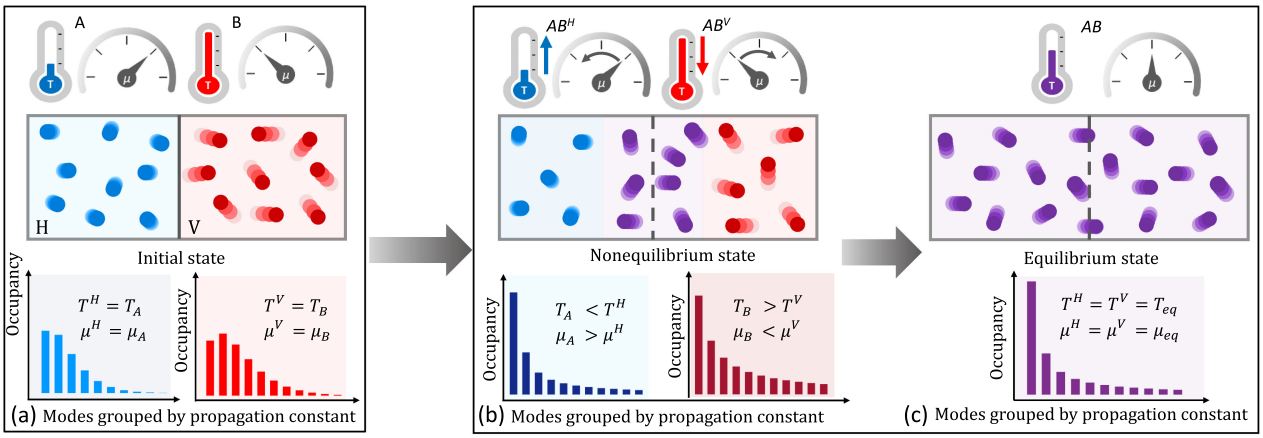

FIG. 1. Sketch of the thermalization process of two photon gases. (a) Initial state: Two orthogonally polarized beams are prepared with different temperatures, chemical potentials, and mode distributions. (b) Nonequilibrium transient state: The difference in temperature and chemical potential among the left and right sides of the box progressively quenches, until their associated mode occupancy progressively approaches the RJ distribution, as a consequence of nonlinear beam propagation, i.e., of heat exchange between the two gases. (c) Equilibrium state: The two gases reach the same values of temperature and chemical potential, and their mode distribution obeys the RJ law.

On the other hand, when placed in the context of calorimetry, temperature acquires a physical connotation. Indeed, when nonequilibrium processes are considered, temperature becomes the physical parameter that governs the exchange of heat (i.e., of energy) between two objects. Specifically, heat can only flow from an object with a higher temperature towards an object with a lower temperature [31]. The heat flow will only stop when a new equilibrium is established, i.e., when both objects have reached the same temperature (T_{eq}).

It is important to underline that such a principle is associated with the maximization of entropy S, i.e., the second law of thermodynamics, whereas the equilibrium statistics of a gas in thermodynamics is only determined by imposing the stationarity of S. Therefore, experimentally demonstrating the establishment of an equilibrium as a consequence of the interaction (heat exchange) between two photon gases is a key for proving that the thermodynamic temperature associated with the RJ mode distribution indeed has a true physical meaning.

In this work, we consider the simplest case of two optical beams (labeled as A and B), which are prepared with different temperatures (T_A and T_B) and chemical potentials (μ_A and μ_B), simultaneously propagating in an MMF. Note that here, by T and μ, we indicate the values of temperature and chemical potential that each gas would reach at thermal equilibrium in the absence of the other gas. In fact, the initial state of both gases is out of equilibrium (see the paragraph below). These results are in accord with previous theoretical predictions where the internal energy U and power P are allowed to resettle between two subsystems [12]. Here, we prepared the two beams with orthogonal vertical and horizontal linear states of polarization, respectively. In this way, the initial state of the system can be depicted as that of two gases that occupy two complementary portions of the total available mode volume [see Fig. 1(a)], corresponding to horizontally and vertically polarized modes. On each side of the box, the color of the beams indicates their temperature. Specifically, the colder gas, depicted in blue, corresponds to the horizontally polarized beam (A), whereas the hotter gas, depicted by red particles, is associated with the vertically polarized beam (B). We note that the use of colors is meant to help visualizing the phenomenon, given that photons belonging to the same mode and polarization are, by nature, fully indistinguishable.

Moreover, note that under sufficiently adiabatic conditions, it is possible to associate a photon gas with a temperature even when the gas is in a nonequilibrium state; i.e., its associated mode occupancy distribution does not yet follow the RJ law, as depicted at the bottom of Fig. 1(a). Indeed, one can compute the value of the temperature on each side of the box in Fig. 1(a) from its corresponding mode occupancy distribution. In fact, although T and μ are defined at thermal equilibrium, their values are not calculated by fitting the RJ distribution at thermal equilibrium. By assuming the presence of negligible linear disorder on short fiber spans, and that T and μ are defined by an RJ modal distribution at thermal equilibrium, their values can be predicted by the mere knowledge of the mode occupancy of the beam at any point of its propagation [19,32] (see Appendix A). Even though the temperature and chemical potential do not possess rigorous physical meaning in exact nonequilibrium processes, they provide general guidelines for the directions of energy and power flows under quasi-equilibrium approximations. Experimentally, we have to measure the power of the laser beam and the mode occupancy at the fiber output. A laser beam

propagating in the MMF core is isolated since the energy losses into the cladding are negligible in the absence of fiber bending [33]. As a consequence, in the presence of a single beam, the nonlinear beam dynamics in an MMF can be described as the free expansion of a gas. This aspect will be of interest in the next sections.

We will use the superscript letters H and V when referring to the parameters of the left and right sides of the box, respectively. On the other hand, when referring to the initial temperature of each gas, we will use as subscripts the letters A and B, respectively. Therefore, the initial state in Fig. 1(a) is defined by $T^H = T_A$, $\mu^H = \mu_A$, $T^V = T_B$, and $\mu^V = \mu_B$.

Once the photon system evolves, the two gases interact, until progressively reaching the same equilibrium parameters. In our picture, the system evolution is enabled by the removal of the barrier between the left and right sides of the box. In particular, it must be noted that removing the barrier allows for the mixing of particles that originally belonged to either the A or the B photon gases. Therefore, it is convenient to describe the thermalization process in terms of the grand canonical ensemble. The chemical potential of each gas will vary: Eventually, as it occurs for the temperature, the chemical potential of the two gases will be the same (μ_{eq}). On the contrary, if the exchange of particles between A and B gases is not allowed, e.g., by means of a barrier that is only permeable to heat, the two gases would remain distinguishable during the whole thermalization process, which would need to be described in terms of the canonical statistical ensemble. In the canonical ensemble regime, each gas subsystem conserves its number of particles during the heat exchange process, and μ^H and μ^V do not converge to the same value at the occurrence of thermalization. In this work, we consider the former case in our experiments. However, we will provide scenarios for possible experimental demonstrations of beam heating and cooling in the framework of a canonical ensemble. We note that, for logistical purposes, we treated the system in a grand canonical ensemble. It is also possible to study the same arrangement in a microcanonical sense, where the total linear momentum and number of photons are conserved.

It is reasonable to assume that the equilibrium value of the temperature and chemical potential [which are associated with violet particles in Figs. 1(b) and 1(c)] is first reached in the center of the box, where the first interactions between the two gases take place [see Fig. 1(b)]. Later, a thermal equilibrium is reached at the box periphery [see Fig. 1(c)]. In its nonequilibrium transient state, each side of the box is associated with a mode distribution that progressively approaches the RJ law [see the histograms at the bottom of Figs. 1(b) and 1(c)]. Of course, as the color map shows, before reaching an equilibrium, the temperatures on the two sides of the box are different. Indeed, in the left part of the box, the coldest gas is still present. As a result, the temperature of the horizontally polarized photon gas will be higher than that of the photons in vertically polarized modes because its associated gas still contains more energetic (red) particles (i.e., $T_A < T^H \leq T^V < T_B$ and $\mu_A > \mu^H \geq \mu^V > \mu_B$). The temperature difference between the left and right sides of the box progressively quenches as the input power grows larger and eventually vanishes when a thermal equilibrium is reached (i.e., $T^H = T^V = T_{\mathrm{eq}}$ and $\mu^H = \mu^V = \mu_{\mathrm{eq}}$). Note that the volume of the box in Fig. 1 must not be confused with that of a classical gas system. Here, in fact, the particles are contained in a "mode" volume, which is not identified by spatial coordinates. In this sense, it is not possible to establish a regime of spatially local equilibrium as is done in nonhomogeneous systems, e.g., when defining the temperature of the surface of the Sun.

The values of T_{eq} and μ_{eq} can be easily calculated. In fact, when a gas of mass $\mathcal{P}$ increases its temperature from $T > 0$ to $T + dT$, it absorbs a quantity of heat δQ, which is given by

$$\delta Q = \mathcal{P} \cdot c \cdot dT, \tag{2}$$

where c is the heat capacity of each gas, which depends on T [34]. However, as it has been demonstrated for an MMF in Ref. [26], when the temperature is sufficiently low, the heat capacity can be treated as a constant, which is the case for our experiments. We underline that the exact values of T_{eq} and μ_{eq} as a result of heat exchange between two gases like in Fig. 1 can be determined by using the same procedure as for a single gas, which is described in Appendix B. In essence, in accordance with the requirement of extensivity, the total energy U, power P, and volume M of the combined system can be obtained through a direct summation of those associated with individual subsystems, i.e., $U = U_A + U_B$, $\mathcal{P} = \mathcal{P}_A + \mathcal{P}_B$, and $M = M_A + M_B$. In the case of two gases interacting in an isolated system, we can impose that $Q_A = -Q_B$, i.e., all of the heat absorbed by A is provided by B, which leads to

$$T_{\mathrm{eq}} = \frac{\mathcal{P}_A T_A + \mathcal{P}_B T_B}{\mathcal{P}_A + \mathcal{P}_B}, \tag{3}$$

where we have reasonably assumed that the two gases have the same heat capacity. Note that Eq. (3) holds as long as both $T_A > 0$ and $T_B > 0$. An exact methodology to predict the final temperature in this composite system is presented in Appendix B. This approach implicitly accounts for the temperature dependence of the optical heat capacities involved. In fact, in the thermodynamic description of multimode optical systems, thermal equilibrium can be reached even at negative temperatures [35,36], which is not within the scope of this study. In addition, it is convenient to define the relative power of the B beam as $R = \mathcal{P}_B/(\mathcal{P}_A + \mathcal{P}_B)$, so that the equilibrium temperature more easily reads as

$T_{eq} = (1-R)T_A + RT_B$. Finally, the value of μ_{eq} can be easily determined by substituting expression (3) in the equation of state (1).

III. EXPERIMENTAL METHODS

Short spans of a graded-index MMF turn out to be the perfect test bed for the verification of the process of heat exchange between two photon gases. In fact, at near-infrared wavelengths, MMFs are an adiabatic system since their optical losses are practically negligible, as long as their length is of the order of a few meters [37] and the beam optical power is far from the catastrophic self-focusing regime [38]. As such, MMFs have been employed for the demonstration of classical wave thermalization [18,19].

Here, we use a 2-m-long span of a standard graded-index MMF (GIF50E from Thorlabs), whose core diameter is 50 μm. Such a fiber supports about 110 modes at the wavelength of our laser (1030 nm, Pharos from Light Conversion, emitting 2-ps pulses with peak powers of the order of tens of kW).

Two laser beams with a transverse diameter of 30 μm are simultaneously injected into the fiber core. The two beams form different small angles (less than 2°) with respect to the fiber axis, in order to be associated with different temperatures. Both beams are injected at the core center. In fact, the presence of both a nonzero injection angle and offset with respect to the fiber axis leads to the impression of an orbital angular momentum, owing to the cylindrical shape of the optical fiber [25], which is responsible for a modification of the equilibrium distribution [32]. In addition, the temperature of beam B is varied by introducing an aperture along the laser path (see Appendix C). The two beams are orthogonally polarized so that any interference at the fiber input facet is avoided: The total power injected into the fiber is simply given by the sum of powers in each of the two beams ($\mathcal{P}_{AB} = \mathcal{P}_A + \mathcal{P}_B$).

At the fiber output, we employed the holographic mode decomposition tool as described in Ref. [30]. This allowed us to retrieve the values of the mode occupancy at the fiber output, permitting us to determine the temperature and chemical potential associated with each photon gas [12].

Finally, let us underline that the propagation distance plays the role of time here. Now, the fiber length is fixed in our experiments, whereas the beam power determines the strength of nonlinear mode mixing, leading to mode energy exchanges within the same beam, or among modes of different beams. Therefore, we may track the "temporal" evolution of the optical temperature in the box as a function of input power [20]. It must be underlined that, as mentioned above, input power also defines the number of photons in a beam. Therefore, in order to emphasize the role of input power in the interaction between different beams (or photon gases), in the following we will refer to the temperature as the ratio between T and $\mathcal{P}$. In this regard, one may notice that this operation does not invalidate the theoretical expectation value of the equilibrium temperature, which only depends on the power ratio between A and B [see Eq. (3)], whose value is fixed in all of our experiments.

IV. SIMPLE CASE OF FREE EXPANSION OF A PHOTON GAS

Let us first consider the simplest case when just a single photon gas is present, which freely expands into a box while doubling its volume [Figs. 2(a) and 2(b)]. This picture corresponds to the injection of a beam that has a horizontal linear polarization at the fiber input, whereas the fiber supports both polarizations. In this case, initially, the gas only occupies half of the whole modal volume, whereas the other half remains empty [Fig. 2(a)]. As a consequence of its nonlinear propagation into the MMF, the beam eventually loses its linear degree of polarization at the fiber output: Modes with vertical polarization also get populated, and the gas uniformly occupies the whole box volume [cf. Fig. 2(b)].

The free expansion of the photon gas can be experimentally demonstrated by projecting the beam at the fiber output onto a given polarization direction by means of a polarizing beam splitter. In particular, as shown in Fig. 2, here we illustrate two significant cases, i.e., corresponding to the insertion of either a vertical or a horizontal barrier in the box. In analogy with Fig. 2(a), a vertical barrier separates the mode volume into horizontally and vertically polarized modes, which are highlighted in Fig. 2(c) by gray and light green colors, respectively, whereas the horizontal barrier projects the modes onto the 45° and the 135° polarization directions, as highlighted in Fig. 2(d) by light blue and yellow colors, respectively.

The intensity profile of the output beam for the four polarization directions is reported in Fig. 2(e). Specifically, these results were obtained when injecting laser pulses of 14 kW of peak power. As can be seen, a bell shape (which is associated with a state of thermal equilibrium) is found along all polarization directions, owing to the occurrence of the beam self-cleaning effect. This finding is in agreement with former studies of the nonlinear polarization dynamics of beam self-cleaning [39]. For the sake of completeness, in Fig. 2(f), we also show the mode distributions associated with the images in Fig. 2(e). Notice that the differences between all of these mode distributions are practically negligible. Thus, they are associated with virtually identical values of T and μ. This result is shown by the data in Fig. 2(g), where we report the values of temperature and chemical potential, which are calculated by starting from the experimental mode decomposition for different projection directions of the output state of polarization. Indeed, the temperature and the chemical potential maintain constant values, within the experimental error.

It is worth noticing that, as mentioned above, one may formally calculate the temperature associated with a

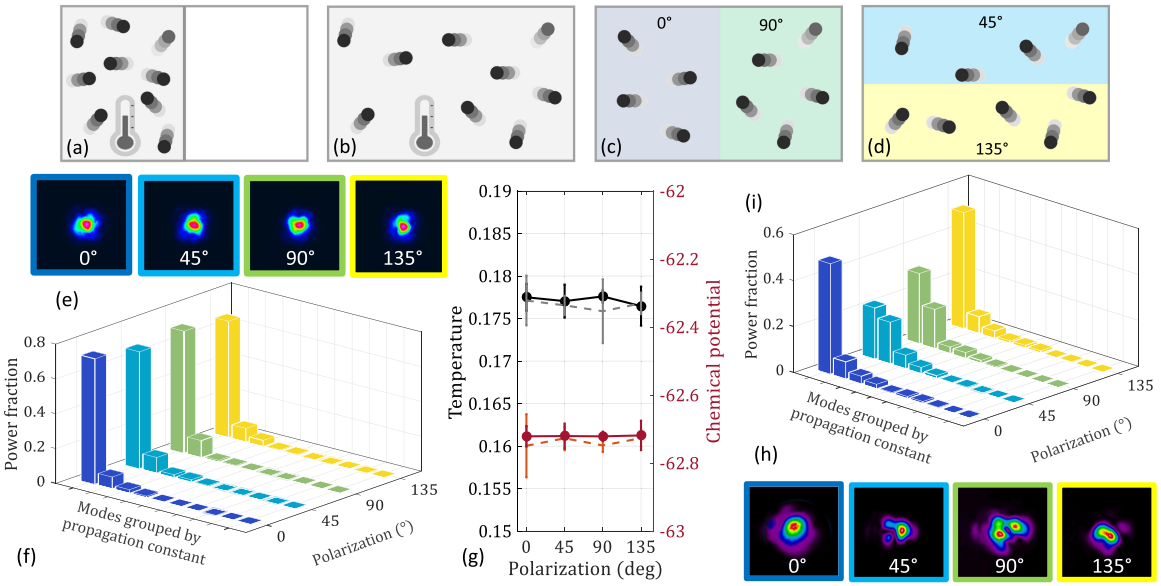

FIG. 2. Free expansion of a photon gas. (a) Input condition associated with a horizontally polarized laser beam. (b) Result of the gas-free expansion. (c),(d) Output polarization analysis corresponding to either horizontal-vertical (c) or $45° - 135°$ (d) polarization splitting. (e) Output beam profiles and (f) their associated normalized mode occupancy (mode power fraction) at an input peak power of 14 kW along different output polarization directions. (g) Temperature and chemical potential associated with the RJ distributions in panel (f). For the error bars, we used the average value of the mode occupancy and its standard deviation, when repeating the same reconstruction algorithm by moving the center of the output beam of ± 1 pixel in each direction with respect to the center position of the CCD camera (see Appendix C for more details). (h),(i) Same as panels (e) and (f) at the input peak power of 7 kW.

speckled beam from its associated mode occupancy values, even if the beam has not yet reached thermal equilibrium. In fact, the thermodynamic parameters are fully defined by the coupling conditions of the laser beam at the fiber input and do not vary as a consequence of the nonlinear propagation of the beam, which is confirmed by the results in Figs. 2(h) and 2(i). These results correspond to a value of the input peak power of 7 kW, which is not high enough for achieving beam self-cleaning along all states of polarization. Indeed, as can be seen in Fig. 2(h), rather different intensity profiles of the output beam are obtained for the four polarization directions. Specifically, the beam only has a bell shape in the horizontal state of polarization, whereas a speckled pattern is found when selecting other polarization directions. As a result, different mode occupancy distributions are found for each output intensity pattern [see Fig. 2(g)]. However, the thermodynamic parameters corresponding to all of these distributions turn out to be exactly the same, in agreement with theoretical expectations.

V. REACHING THERMAL EQUILIBRIUM WHEN MIXING TWO PHOTON GASES WITH THE SAME "MASS"

In this section, we consider the thermalization process of two beams carrying the same power (i.e., $R = 1/2$). Correspondingly, the two gases are formed by the same number of particles; i.e., they have the same "mass." Aiming at emphasizing the role of heat exchange between the two gases, we compare three different injection conditions. Specifically, we consider the injection of the sole A beam, the injection of the sole B beam, and the injection of both beams. In order to distinguish the corresponding thermodynamic parameters, in the following, these three cases will be associated with the subscript symbols A, B, and AB, respectively (e.g., the temperature of the left side of the box when only the A beam is present will be referred to as T_A^H).

The experimental results, in this case, are shown in Fig. 3. At first, we inserted a horizontal-vertical beam splitter at the fiber output, which is analogous to inserting a vertical barrier into the box, as depicted in Fig. 3(a). The corresponding values of the temperature and the chemical potential at both sides of the box are shown in Figs. 3(b) and 3(c) (see Appendix A for details about the calculation of thermodynamic parameters). In agreement with theoretical expectations, we found that, in the presence of both beams, the temperature at the left side of the box is always higher than the temperature measured in the presence of the sole A beam, for all values of the input power, i.e., $T_A^H \geq T_{AB}^H$. On the contrary, symmetrically, we have that $T_B^V \geq T_{AB}^V$ ($\mu_B^V \leq \mu_{AB}^V$). In particular, at low input powers, i.e., in the quasilinear regime, the temperature at the left side of the box remains the same, within the experimental error, independently of whether we inject the sole A beam, or both the A and B beams ($T_A^H \simeq T_{AB}^H$). On the contrary, as the input power grows larger, the T_{AB}^H curve progressively

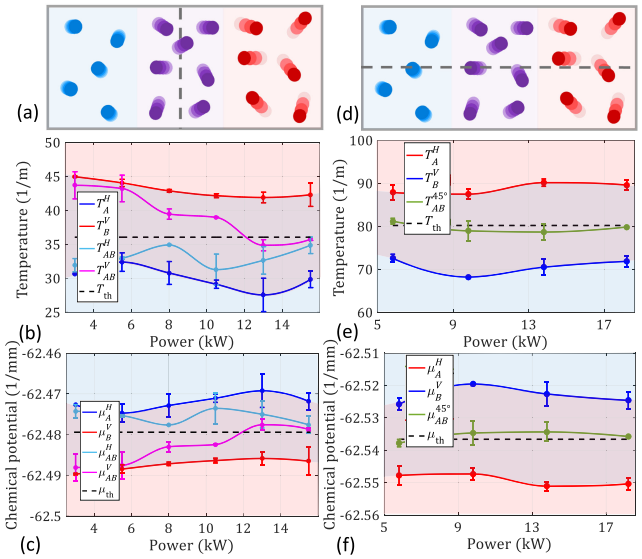

FIG. 3. Thermal equilibrium in the presence of two photon gases with the same mass ($R = 1/2$). (a)–(c) Schematic representation of polarization analysis corresponding to horizontal-vertical polarization splitting (a), and corresponding measured values of temperature (b) and chemical potential (c), either in the presence of the sole A and B beams or when simultaneously injecting A and B beams into the MMF core. (d)–(f) Same as panels (a)–(c) for $45° - 135°$ polarization splitting. The solid lines in panels (b), (c), (e), and (f) are guides for the eye. For the error bars, we used the average value of the mode occupancy and its standard deviation when repeating the same reconstruction algorithm by moving the center of the output beam of ± 1 pixel in each direction with respect to the center position of the CCD camera (see Appendix C for more details).

drops down until it reaches a plateau value, which coincides with that of T^V_{AB}, i.e., the temperature at the right side of the box, that is obtained when both the A and B beams copropagate into the MMF. This finding indicates that an equilibrium temperature is reached, whose value is in good agreement with the theoretical expectation of Eq. (3) [dashed black line in Fig. 3(b)].

It is worth noting that the temperature at both sides of the box does not vary with input power in the case where only one beam is present; i.e., both the T^H_A and T^V_B curves are flat in Fig. 3(b). This finding confirms that the nonlinear beam dynamics in an MMF can indeed be described as the free expansion of a gas, as discussed in the previous section. In order to clarify the connection with the mode occupancy distribution shown in Fig. 2, we report in Appendix D the mode occupancy distributions relative to the experiments in Figs. 3(a)–3(c).

The evolution of the chemical potential follows the same trend of the gas temperature. In Fig. 3(c), we can see that μ^H_{AB} and μ^V_{AB} both reach the same value at high input powers, whereas at low input powers, their values are close to that of μ^H_A and μ^V_B, respectively. This further proves that a thermalization phenomenon between two indistinguishable gases is observed. In this regard, it is worth mentioning that distinguishing the beams through their polarization state was the easiest solution that could be adopted with our experimental setup. Nevertheless, the theoretical principle behind beam cooling and heating goes beyond this specific case. For example, one may think of using two beams emitted by laser sources that differ in their wavelength or pulse duration, thus enabling the observation of thermalization within the canonical ensemble. In this sense, it is worth mentioning that studies of wave thermalization of orthogonally polarized beams have been carried out in Refs. [40,41], albeit in the frequency domain with either highly birefringent or polarization-maintaining single-mode fibers, respectively.

In order to further confirm the validity of the representation in Fig. 1, we analyzed the output beam projections along the $45° - 135°$ polarization directions. Indeed, if the representations in Fig. 3(a) are valid, one would expect to observe a temperature in the upper and lower sides of the box which does not depend on input power. The average temperature of the top and bottom sides of the box in Fig. 3(d) is expected to be the same, since both sides contain the same amount of hot, cold, and thermalized particles, although the system is clearly not yet at equilibrium. This is in agreement with the experimental results reported in Figs. 3(e) and 3(f), where we show that both temperature and chemical potential obtained when simultaneously injecting A and B beams maintain nearly constant values as the input power is varied. Such behavior is the opposite of what is observed in Figs. 3(b) and 3(c), thus validating our model of gas thermalization, which is illustrated in Fig. 1. As a final note, we highlight that the values of T and μ in Figs. 3(b)–3(c) and Figs. 3(e)–3(f) are different, simply because the experimental results reported therein were carried out on different days, i.e., with different experimental input laser-fiber coupling conditions.

VI. ENTROPY GROWTH

One may notice that in Fig. 3(a), we are neglecting the spreading of the red gas into the right side of the box [as depicted in Figs. 2(a) and 2(b)]. In this regard, it must be emphasized that the results in Figs. 3(b) and 3(c) demonstrate that, even if present, the spreading of the gases into opposite sides of the box is a slower process when compared with the change of temperature of their particles. In other words, the energy exchange between modes is a more efficient process than nonlinear depolarization. Moreover, the possible spreading of nonthermalized particles on the opposite side of the box, e.g., that given by linear depolarization, would not invalidate the theory of photon beam calorimetry. Indeed, the establishment of the equilibrium is not only determined by the measurement of one and the same temperature. Thermal equilibrium is properly reached if and only if the mode occupancy

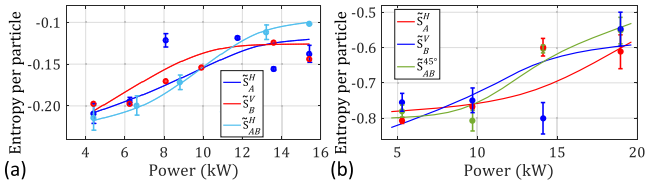

FIG. 4. Experimental demonstration of the entropy growth. (a), (b) Values of the entropy calculated from the data in Figs. 3(b) and 3(c) and Figs. 3(e) and 3(f), respectively, either in the presence of the sole A or B beam or when simultaneously injecting both A and B beams into the fiber, taking the projection on the horizontal direction (a) and on the direction at 45° with the fiber axes (b), respectively. The curves are simply guides for the eye. For the error bars, we used the average value of the mode occupancy and its standard deviation when repeating the same reconstruction algorithm by moving the center of the output beam of ± 1 pixel in each direction with respect to the center position of the CCD camera (see Appendix C for more details).

distribution on the left and right sides of the box is identical, and it follows the RJ law, i.e., only if the entropy has reached a maximum. This result has been experimentally verified (see Appendix D). Indeed, we found that only at the highest value of the input power (i.e., 16 kW) the distribution associated with both horizontally and vertically polarized modes properly obeys the RJ law.

At the same time, we verified the crucial condition that entropy grows larger when the input power grows larger. In particular, in Figs. 4(a) and 4(b), we illustrate the measured variation of entropy with input laser power, corresponding to experimental results in Figs. 3(b) and 3(c) and Figs. 3(e) and 3(f), respectively. Following the methods of Ref. [12], the entropy can be calculated as

$$S = \sum_{i=1}^{M} \ln n_i, \tag{4}$$

where the index i runs over all modes, whose occupancy is indicated as n_i. Further details on the method for computing the entropy are reported in Appendix A. We note that the entropy provided by Eq. (4) can be formally derived from the Gibbs-Shannon entropy when the modal occupancies are very high [16] and is therefore compatible with the H-theorem of entropy growth [42]. Moreover, being an extensive variable, the entropy explicitly depends on the power. In order to evaluate the contribution to the entropy given by the mode power variation during propagation, we will consider the entropy per particle $\tilde{S}$, which is defined as

$$\tilde{S} = \sum_{i=1}^{N} \ln |c_i|^2, \tag{5}$$

where $|c_i|^2$ is the normalized power fraction of the ith mode. Note that if $\tilde{S}$ grows with the power, so does the entropy S. Therefore, verifying the growth of $\tilde{S}$ with power is sufficient to demonstrate the increase of entropy as a consequence of the thermalization process upon propagation.

As can be seen in Figs. 4(a) and 4(b), in all cases the entropy per particle clearly experiences growth when moving from low to high input powers, i.e., from an out-of-equilibrium state to a state of full thermal equilibrium. In particular, the green curve in Fig. 4(b) indicates that, although its temperature is equal to T_{eq} [cf. Fig. 3(e)], thermal equilibrium in the top side of the box in Fig. 3(d) is not reached at low powers since its associated entropy is not maximized yet. This finding further confirms that, even if present, effects responsible for the diffusion of a gas into the whole modal volume, i.e., linear or nonlinear depolarization, cannot force the system to reach thermal equilibrium: It can only be reached thanks to heat exchange between the two gases.

VII. HOW TO TUNE EQUILIBRIUM TEMPERATURE

Finally, let us demonstrate how it is possible to control the equilibrium temperature of the gas mixture.

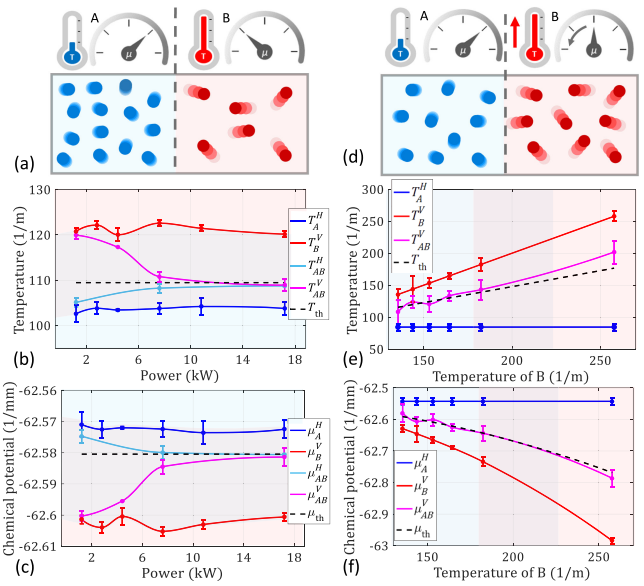

FIG. 5. Tuning of the equilibrium temperature of interacting photon gases. (a)–(c) Same as Fig. 3, when setting $R = 1/3$. (d) Sketch of the input state when varying T_B with respect to Fig. 3(a). (e),(f) Variation of the temperatures (e) and chemical potentials (f) at the left and right sides of the box vs T_B. In order to ensure system thermalization, in panels (e) and (f), the input power is equal to 16 kW, and $R = 1/2$. The solid lines in panels (b), (c), (e), and (f) are guides for the eye. For the error bars, we used the average value of the mode occupancy and its standard deviation, when repeating the same reconstruction algorithm by moving the center of the output beam of ± 1 pixel in each direction with respect to the center position of the CCD camera (see Appendix C for more details).

By recalling Eq. (3), it appears evident that there are only two ways of tuning the equilibrium temperature, i.e., by acting on either R or on the initial temperature of the two gases. Here, we experimentally demonstrate both these possibilities, as illustrated in Figs. 5(a)–5(c) and 5(d)–5(f), respectively. In Figs. 5(b) and 5(c), we report the results of the same experiment that was shown in Figs. 3(b) and 3(c), but now setting $R = 1/3$. As can be seen, even in this case, there is good agreement between the experimental results and the theoretical expectations (black dashed curve). The equilibrium temperature is closer to that of the gas with the higher mass (B), as it occurs for gases made of matter particles. Finally, we vary the temperature of beam B (T_B) while keeping its associated number of particles constant. In Fig. 5(e), we show that the equilibrium temperature linearly scales with T_B, as expected from theory. In particular, in the experiment reported in Fig. 5(e), we prepare the beams so that $R = 1/2$: Here, the input power is high enough to ensure full gas thermalization [as in Fig. 1(c)], except for the point corresponding to the highest value of T_B. Clearly, the theoretical value of the thermal equilibrium temperature of the gas mixture is always found at the midpoint between T_A and T_B. Analogously, the chemical potential of the mixture is the average of the chemical potentials of the A and B beams [cf. Fig. 5(f)].

VIII. CONCLUSION

By employing calorimetric methods, we have experimentally demonstrated the exchange of both power and energy between the two polarization-mode groups supported by a nonlinear optical multimode fiber. These observations confirm that the thermodynamic parameters T and μ represent meaningful thermodynamic forces that govern the direction of flow of their respective conjugate parameters. Indeed, our experimental results unambiguously prove that the statistical mechanics framework previously developed to describe the utterly complex dynamics in nonlinear optical multimode systems respects the thermodynamics principles of energy conservation and entropy growth. In this work, we have shown that the "heat" transfer (ΔU) between two orthogonally polarized beams unfolds as expected in a grand canonical ensemble. Our work may pave the way for demonstrating similar results in canonical-like systems where power exchange is forbidden. It would be of interest to investigate whether similar schemes can be used for beam-quality-improvement applications and for developing high-power fiber lasers.

ACKNOWLEDGMENTS

M. F., F. M., and S. W. acknowledge NextGenerationEU, partnership on "Telecommunications of the Future" (PE00000001—program "RESTART"), and Sapienza University (Grants No. RG12117A84DA7437, No. SP12218480C7D1E9, and No. AR2221815ED243A0). The work of D. N. C. was partially supported by Air Force Office of Scientific Research (MURI: FA9550-20-1-0322, S004112), Office of Naval Research (MURI: N00014-20-1-2789), Army Research Office (W911NF-23-1-0312), Israel Ministry of Defense (IMOD: 4441279927), National Science Foundation (CCF-2320937), and MPS Simons collaboration (Simons grant 733682). All authors acknowledge D. S. Kharenko, M. Gervaziev, and Y. Sun for helping in the development of the mode decomposition setup.

The authors declare no conflicts of interest.

APPENDIX A: CALCULATION OF THERMODYNAMIC PARAMETERS FROM EXPERIMENTAL DATA

The Boltzmann entropy is defined as

$$S = \ln W, \tag{A1}$$

where W for bosonic systems can be written as [12]

$$W(\{n_i\}) = \prod_{i=1}^{M} \frac{(n_i + g_i - 1)!}{n_i!(g_i - 1)!}. \tag{A2}$$

Here, the index i is used for grouping all the degenerate g_i modes, having the same propagation constant, with photon occupancy n_i. Note that, in our MD experiments, we measured the power fraction associated with each mode, which is directly proportional to n_i. Therefore, in practice, we consider n_i to be a power fraction since the proportionality constant will only provide a (superfluous) additional term in Eq. (A1).

It is evident that the terms in Eq. (A2) for which $n_i = 0$ do not contribute to the product since they are equal to 1. Therefore, the entropy can be written as

$$S = \sum_{i|n_i \neq 0} \ln \frac{(n_i + g_i - 1)!}{n_i!(g_i - 1)!}, \tag{A3}$$

which, following the same derivation of Ref. [12], leads to

$$S = \sum_{i|n_i \neq 0} \ln n_i, \tag{A4}$$

or equivalently

$$S = \sum_i S_i, \tag{A5}$$

where

$$S_i = \begin{cases} \ln n_i & \text{if } n_i \neq 0 \\ 0 & \text{if } n_i = 0. \end{cases} \tag{A6}$$

Experimentally, we often found that some modes have a power fraction close to zero, which makes the logarithmic term in Eq. (A6) diverge. For instance, when dealing with thermalized beams, high-order modes are associated with power fractions that are quickly damped when the index i grows larger, as predicted by the RJ distribution. Therefore, in order to meaningfully evaluate the entropy, it is necessary to take into account the tolerances that are imposed by the limited accuracy of our MD. In particular, we call Δn the experimental error of our MD method for the estimate of the mode occupancy, and we consider

$$S_i = \begin{cases} \ln n_i & \text{if } n_i \gtrsim \Delta n \\ 0 & \text{if } n_i \lesssim \Delta n. \end{cases} \tag{A7}$$

Specifically, in the plots of Fig. 4 of the main text, we have set $\Delta n = 0.08$, whereas the experimental results shown in all other figures take into account the occupancy of all modes. This is because the condition $n_i = 0$ is not detrimental for the accurate estimation of any thermodynamic parameter, except for S.

The values of T and μ were calculated as described in Ref. [12]: The definition of the total optical power, i.e.,

$$\mathcal{P} = \sum_i n_i, \tag{A8}$$

and that of the internal energy, i.e.,

$$U = \sum_i \beta_i n_i, \tag{A9}$$

where β_i is the propagation constant of the ith mode, are used in the equation of state [i.e., Eq. (1) in the main text] $U - \mu\mathcal{P} = MT$. This result provides an equation with two unknowns (T and μ), which, combined with the RJ law, i.e.,

$$\frac{n_i}{g_i} = -\frac{T}{\mu + \beta_i}, \tag{A10}$$

leads to a nonlinear system of equations that has a unique solution for T and μ, as long as the physical condition $n_i \geq 0$ is imposed [12].

APPENDIX B: RIGOROUS PREDICTION OF EQUILIBRIUM TEMPERATURE

In a grand-canonical-like system, from the initial conditions, the final temperature and chemical potential can be rigorously predicted by treating the whole system as a microcanonical-like system. In doing so, the energy levels β, power $\mathcal{P}$, and optical energy U of the subsystems A and B are combined into the total energy levels $\beta_T = \beta_A \uplus \beta_B$, the total power $\mathcal{P}_T = \mathcal{P}_A + \mathcal{P}_B$, and the total optical energy $U_T = U_A + U_B$. The final temperature is obtained by matching the conservation laws [13]. The temperature obtained by this method implicitly accounts for the temperature dependence of the heat capacities involved, and Eq. (3) in the main text is a valid approximation of the rigorous method as long as the two optical temperatures are relatively close to each other, as shown in Fig. 6.

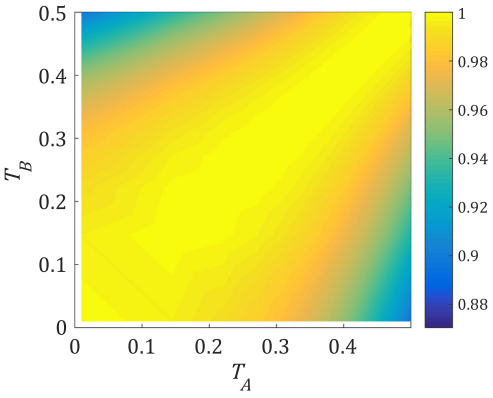

FIG. 6. Ratio of the temperature obtained rigorously to the temperature obtained by Eq. (3) under various initial T_A and T_B of the subsystems. This plot is obtained when $\mathcal{P}_A = \mathcal{P}_B = 1$.

APPENDIX C: PREPARATION OF THE GAS INITIAL STATE

Our experimental setup is shown in Fig. 7. Experiments were carried out by means of a Yb-based laser system (Light Conversion PHAROS-SP-HP), generating pulses of 2 ps with a 100-kHz repetition rate, at 1030 nm. The temporal profile of the laser pulses is averaged by the mode decomposition tool. Such an average operation lies at the base of the statistical mechanics approach. As has been demonstrated by Leventoux *et al.*, in fact, at the occurrence of self-cleaning, the beam spatial profile strongly differs when considering the peak and the tails of the pulse [43]. The cleaning effect is the result of an average process; thus, it can be described as a process of wave thermalization. In this regard, it has to be mentioned that other demonstrations

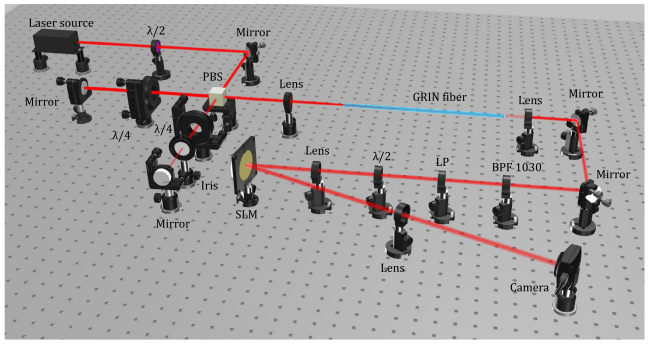

FIG. 7. Sketch of the experimental setup. $\lambda/2$: half-wave plate; $\lambda/4$: quarter-wave plate; PBS: polarizing beam splitter; BPF 1030: band pass filter at 1030 nm; LP: linear polarizer; SLM: spatial light modulator.

of beam self-cleaning exploited, instead, the average over several input conditions corresponding to nearly the same values of $\mathcal{P}$ and U [26]. By means of a polarizing beam splitter, we separate the laser beam into an interferometer-like path, where each arm corresponds to a photon gas, as depicted in Fig. 1 of the main text. The setup is built in order to ensure that, once recombined, the two beams are temporally synchronized and with orthogonal linear states of polarization. The mirrors of one of the two arms is slightly tilted. In this way, we can prepare the two beams with different photon gas temperatures. The tilting angle is about 2°. We verified that introducing such an angle does not alter the transmitted power; i.e., the injection efficiency remains virtually the same. However, the intensity profile (at low powers) at the output of the fiber, as well as its associated value of temperature, can be significantly modified.

The power ratio R between the two beams at the fiber input is determined by the orientation of a half-wave plate, which is placed upstream of the beam splitter, whereas the variation of T_B, which we describe in Figs. 5(d)–5(f) in the main text, is possible by means of an iris placed in arm B (see Fig. 7). The iris distorts the wavefront of the B beam, thus varying its associated temperature. Indeed, acting on the wavefront shape permits us to modify the mode distribution (and, consequently, the thermodynamic parameters) associated with the initial state. However, the iris is also responsible for a loss of beam power, i.e., for the reduction of the mass of gas B. In order to ensure that the value of R remains the same in the experiments of Fig. 5 of the main text, we compensate the power lost because of the iris by means of a quarter-wave plate, inserted in cascade with the iris (see Fig. 7). Note that another quarter-wave plate was placed in arm A. This is because, in the absence of the quarter-wave plates, no light would reach the input tip of the MMF, since both arms would maintain their state of polarization, thus would be reflected back towards the laser source by the polarizing beam splitter.

At the fiber output, the beam was collected by means of a lens and analyzed by means of a MD setup, consisting of a bandpass filter, a polarizer (or, equivalently, a polarizing beam splitter), a half-wave plate, two lenses, a spatial light modulator (Hamamatsu LCOS- X15213), and a CCD camera (Gentec Beamage-4M-IR). The working mechanism of the MD setup has been discussed in full detail elsewhere; see, for example, Ref. [30]. Here, we limit ourselves to recalling that the main source of error of our MD is due to the association between the center of the beam at the fiber output with that of the spatial light modulator. This is at the origin of the error bars that are associated with the thermodynamic parameters in the figures of the main text. Specifically, for each experiment at given input power and injection conditions, we identify the center of the beam with a certain pixel of the CCD camera. Then, we run the same reconstruction algorithm by moving the center of the beam by ± 1 pixel in each direction. This process provides us with a set of nine different values of the mode occupancy, which are used to estimate the error on T and μ. Further details on the estimation of the error can be found in Ref. [19].

APPENDIX D: MODE EQUILIBRIUM DISTRIBUTION

In Fig. 8, we report the experimental mode distribution that corresponds to the data shown in Figs. 3(a)–3(c) of the main text. For the sake of simplicity, we only show results obtained for the lowest (left column) and for the highest (right column) values of input power, i.e., corresponding to either a nonequilibrium or to a thermal equilibrium state, respectively. In each subfigure, we plot as a colored histogram the experimental mode power distribution, whereas the dashed black lines illustrate their associated equilibrium RJ distribution. As can be seen, at the highest powers, the histogram bars are well fitted by the RJ law. On the contrary, at low powers, when thermal equilibrium has not yet been reached, there is a clear discrepancy between the experimental data and the RJ law. We underline that the y axis of the plots in Fig. 8 represents the power fraction in each mode within a group with degeneracy g_i, whereas in our former work (Ref. [19]),

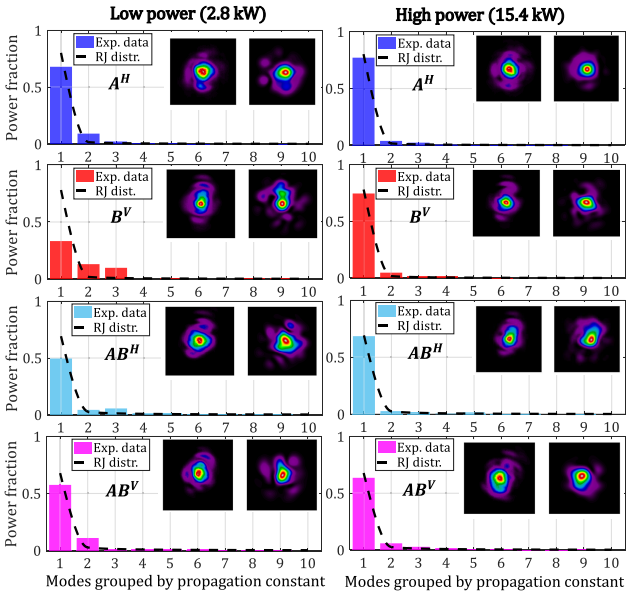

FIG. 8. MD of the output beam corresponding to the experiments in Figs. 3(a)–3(c) (main text), when operating either in the linear (left column) or in the nonlinear (right column) beam propagation regime, i.e., at 2.8 kW and 15.4 kW, respectively. The inset pictures show the measured intensity of the near field (left) and the holographic reconstructions (right). The four rows represent different input conditions, i.e., either in the presence of the sole A (blue bars) and B (red bars) beams, or when simultaneously injecting both A and B beams (azure and purple bars) into the MMF core, respectively.

TABLE I. Computed RMSE between the experimental mode decomposition data in Fig. 8 and their associated theoretical RJ curves.

	Lowest power	Highest power
RMSE_{A^H}	4.0%	3.5%
RMSE_{B^V}	8.0%	3.5%
RMSE_{AB^H}	3.4%	2.9%
RMSE_{AB^V}	3.8%	3.0%

we used it to plot the total power of each mode group. Finally, in order to highlight the good quantitative agreement between theory and experiments, we computed the root-mean-square error (RMSE) between the experimental data and the theoretical RJ distribution. The RMSE values associated with the plots in Fig. 8 are reported in Table I.

[1] T. Byrnes, N. Y. Kim, and Y. Yamamoto, *Exciton–polariton condensates*, Nat. Phys. **10**, 803 (2014).

[2] J. Klaers, J. Schmitt, F. Vewinger, and M. Weitz, *Bose–Einstein condensation of photons in an optical microcavity*, Nature (London) **468**, 545 (2010).

[3] G. Baffou and R. Quidant, *Thermo-plasmonics: Using metallic nanostructures as nano-sources of heat*, Laser Photonics Rev. **7**, 171 (2013).

[4] R. W. Boyd, *Nonlinear Optics* (Academic Press, New York, 2020).

[5] M. Onorato, L. Vozella, D. Proment, and Y. V. Lvov, *Route to thermalization in the α-Fermi–Pasta–Ulam system*, Proc. Natl. Acad. Sci. U.S.A. **112**, 4208 (2015).

[6] A. Picozzi, J. Garnier, T. Hansson, P. Suret, S. Randoux, G. Millot, and D. N. Christodoulides, *Optical wave turbulence: Towards a unified nonequilibrium thermodynamic formulation of statistical nonlinear optics*, Phys. Rep. **542**, 1 (2014).

[7] M. Guasoni, J. Garnier, B. Rumpf, D. Sugny, J. Fatome, F. Amrani, G. Millot, and A. Picozzi, *Incoherent Fermi-Pasta-Ulam recurrences and unconstrained thermalization mediated by strong phase correlations*, Phys. Rev. X **7**, 011025 (2017).

[8] D. Pierangeli, M. Flammini, L. Zhang, G. Marcucci, A. Agranat, P. Grinevich, P. Santini, C. Conti, and E. DelRe, *Observation of Fermi-Pasta-Ulam-Tsingou recurrence and its exact dynamics*, Phys. Rev. X **8**, 041017 (2018).

[9] B. Barviau, B. Kibler, S. Coen, and A. Picozzi, *Toward a thermodynamic description of supercontinuum generation*, Opt. Lett. **33**, 2833 (2008).

[10] G. Vanderhaegen, P. Szriftgiser, A. Kudlinski, M. Conforti, A. Armaroli, and A. Mussot, *Observation of the noise-driven thermalization of the Fermi-Pasta-Ulam-Tsingou recurrence in optical fibers*, Phys. Rev. A **106**, 033519 (2022).

[11] N. Berti, K. Baudin, A. Fusaro, G. Millot, A. Picozzi, and J. Garnier, *Interplay of thermalization and strong disorder: Wave turbulence theory, numerical simulations, and experiments in multimode optical fibers*, Phys. Rev. Lett. **129**, 063901 (2022).

[12] F. O. Wu, A. U. Hassan, and D. N. Christodoulides, *Thermodynamic theory of highly multimoded nonlinear optical systems*, Nat. Photonics **13**, 776 (2019).

[13] M. Parto, F. O. Wu, P. S. Jung, K. Makris, and D. N. Christodoulides, *Thermodynamic conditions governing the optical temperature and chemical potential in nonlinear highly multimoded photonic systems*, Opt. Lett. **44**, 3936 (2019).

[14] M. Ferraro, F. Mangini, M. Zitelli, and S. Wabnitz, *On spatial beam self-cleaning from the perspective of optical wave thermalization in multimode graded-index fibers*, Adv. Phys. X **8**, 2228018 (2023).

[15] E. Busley, L. E. Miranda, A. Redmann, C. Kurtscheid, K. K. Umesh, F. Vewinger, M. Weitz, and J. Schmitt, *Compressibility and the equation of state of an optical quantum gas in a box*, Science **375**, 1403 (2022).

[16] K. G. Makris, F. O. Wu, P. S. Jung, and D. N. Christodoulides, *Statistical mechanics of weakly nonlinear optical multimode gases*, Opt. Lett. **45**, 1651 (2020).

[17] Q. Zhong, F. O. Wu, A. U. Hassan, R. El-Ganainy, and D. N. Christodoulides, *Universality of light thermalization in multimoded nonlinear optical systems*, Nat. Commun. **14**, 370 (2023).

[18] H. Pourbeyram, P. Sidorenko, F. O. Wu, N. Bender, L. Wright, D. N. Christodoulides, and F. Wise, *Direct observations of thermalization to a Rayleigh–Jeans Distribution in Multimode Optical Fibres*, Nat. Phys. **18**, 685 (2022).

[19] F. Mangini, M. Gervaziev, M. Ferraro, D. Kharenko, M. Zitelli, Y. Sun, V. Couderc, E. Podivilov, S. Babin, and S. Wabnitz, *Statistical mechanics of beam self-cleaning in grin multimode optical fibers*, Opt. Express **30**, 10850 (2022).

[20] K. Krupa, A. Tonello, B. M. Shalaby, M. Fabert, A. Barthélémy, G. Millot, S. Wabnitz, and V. Couderc, *Spatial beam self-cleaning in multimode fibres*, Nat. Photonics **11**, 237 (2017).

[21] Z. Liu, L. G. Wright, D. N. Christodoulides, and F. W. Wise, *Kerr self-cleaning of femtosecond-pulsed beams in graded-index multimode fiber*, Opt. Lett. **41**, 3675 (2016).

[22] L. G. Wright, D. N. Christodoulides, and F. W. Wise, *Spatiotemporal mode-locking in multimode fiber lasers*, Science **358**, 94 (2017).

[23] U. Tegin, B. Rahmani, E. Kakkava, D. Psaltis, and C. Moser, *Single-mode output by controlling the spatiotemporal nonlinearities in mode-locked femtosecond multimode fiber lasers*, Adv. Opt. Photonics **2**, 056005 (2020).

[24] N. O. Moussa, T. Mansuryan, C.-H. Hage, M. Fabert, K. Krupa, A. Tonello, M. Ferraro, L. Leggio, M. Zitelli, F. Mangini *et al.*, *Spatiotemporal beam self-cleaning for high-resolution nonlinear fluorescence imaging with multimode fiber*, Sci. Rep. **11**, 18240 (2021).

[25] E. Podivilov, F. Mangini, O. Sidelnikov, M. Ferraro, M. Gervaziev, D. Kharenko, M. Zitelli, M. Fedoruk, S. Babin, and S. Wabnitz, *Thermalization of orbital angular momentum beams in multimode optical fibers*, Phys. Rev. Lett. **128**, 243901 (2022).

[26] K. Baudin, A. Fusaro, K. Krupa, J. Garnier, S. Rica, G. Millot, and A. Picozzi, *Classical Rayleigh-Jeans*

condensation of light waves: Observation and thermodynamic characterization, Phys. Rev. Lett. **125**, 244101 (2020).
[27] C. Connaughton, C. Josserand, A. Picozzi, Y. Pomeau, and S. Rica, *Condensation of classical nonlinear waves*, Phys. Rev. Lett. **95**, 263901 (2005).
[28] P. Aschieri, J. Garnier, C. Michel, V. Doya, and A. Picozzi, *Condensation and thermalization of classical optical waves in a waveguide*, Phys. Rev. A **83**, 033838 (2011).
[29] T. Damm, J. Schmitt, Q. Liang, D. Dung, F. Vewinger, M. Weitz, and J. Klaers, *Calorimetry of a Bose–Einstein-condensed photon gas*, Nat. Commun. **7**, 11340 (2016).
[30] M. Gervaziev, I. Zhdanov, D. Kharenko, V. Gonta, V. Volosi, E. Podivilov, S. Babin, and S. Wabnitz, *Mode decomposition of multimode optical fiber beams by phase-only spatial light modulator*, Laser Phys. Lett. **18**, 015101 (2020).
[31] E. Fermi, *Thermodynamics* (Dover Publications, Inc., Mineola, NY, 2012).
[32] F. O. Wu, Q. Zhong, H. Ren, P. S. Jung, K. G. Makris, and D. N. Christodoulides, *Thermalization of light's orbital angular momentum in nonlinear multimode waveguide systems*, Phys. Rev. Lett. **128**, 123901 (2022).
[33] D. Gloge, *Bending loss in multimode fibers with graded and ungraded core index*, Appl. Opt. **11**, 2506 (1972).
[34] F. O. Wu, P. S. Jung, M. Parto, M. Khajavikhan, and D. N. Christodoulides, *Entropic thermodynamics of nonlinear photonic chain networks*, Commun. Phys. **3**, 216 (2020).
[35] A. Marques Muniz, F. Wu, P. Jung, M. Khajavikhan, D. Christodoulides, and U. Peschel, *Observation of photon-photon thermodynamic processes under negative optical temperature conditions*, Science **379**, 1019 (2023).
[36] K. Baudin, J. Garnier, A. Fusaro, N. Berti, C. Michel, K. Krupa, G. Millot, and A. Picozzi, *Observation of light thermalization to negative-temperature Rayleigh-Jeans equilibrium states in multimode optical fibers*, Phys. Rev. Lett. **130**, 063801 (2023).
[37] G. P. Agrawal, *Nonlinear fiber optics*, in *Nonlinear Science at the Dawn of the 21st Century* (Springer, New York, 2000), pp. 195–211.
[38] M. Ferraro, F. Mangini, M. Zitelli, A. Tonello, A. De Luca, V. Couderc, and S. Wabnitz, *Femtosecond nonlinear losses in multimode optical fibers*, Photonics Research **9**, 2443 (2021).
[39] K. Krupa, G. G. Castañeda, A. Tonello, A. Niang, D. S. Kharenko, M. Fabert, V. Couderc, G. Millot, U. Minoni, D. Modotto *et al.*, *Nonlinear polarization dynamics of Kerr beam self-cleaning in a graded-index multimode optical fiber*, Opt. Lett. **44**, 171 (2019).
[40] S. Pitois, S. Lagrange, H. R. Jauslin, and A. Picozzi, *Velocity locking of incoherent nonlinear wave packets*, Phys. Rev. Lett. **97**, 033902 (2006).
[41] P. Suret, S. Randoux, H. R. Jauslin, and A. Picozzi, *Anomalous thermalization of nonlinear wave systems*, Phys. Rev. Lett. **104**, 054101 (2010).
[42] A. Fusaro, J. Garnier, K. Krupa, G. Millot, and A. Picozzi, *Dramatic acceleration of wave condensation mediated by disorder in multimode fibers*, Phys. Rev. Lett. **122**, 123902 (2019).
[43] Y. Leventoux, G. Granger, K. Krupa, A. Tonello, G. Millot, M. Ferraro, F. Mangini, M. Zitelli, S. Wabnitz, S. Février *et al.*, *3D time-domain beam mapping for studying nonlinear dynamics in multimode optical fibers*, Opt. Lett. **46**, 66 (2021).